Supplementary Materials and methods

1 Mathematical model

We use a computational hybrid model based on that presented in McLennan et al. (2012, 2015a,b, 2017). The model is a two-dimensional approximation of the system and consists of a discrete, off-lattice model for the dynamics of neural crest cells that is coupled to a continuum, reaction-diffusion model for the dynamics of chemoattractant (VEGF). We implement the model using Aboria (Robinson, 2017, https://martinjrobins.github.io/Aboria/), a C++ library for particle-based numerical methods.

1.1 Dynamics of cells

We describe briefly how we incorporate the dynamics of cells. We assume that there are two types of cells, namely "leaders" and "followers". Leaders undertake a fixed-jump-length biased random walk up a cell-induced gradient of chemoattractant. To model the cells extending filopodia to sense the concentration of chemoattracant at their tips we simply sample the concentration at a certain number of points a fixed distance away from the center of a cell in randomly chosen directions, and then move the cell in the direction of the highest concentration sensed, provided it is sufficiently higher than the chemoattractant concentration at the position of the center of the cell. If this is not the case, we move the cell in a random direction. On the other hand, followers are either in chains or they move randomly. A chain consists of a group of followers that are close to each other, with at least one of them close to a leader. All the followers in a chain move in the same direction as the leader that is at the front of that chain. If a follower is able to follow more than one cell, i.e. it could join multiple chains, it randomly chooses one to join.

In addition to this model of cell guidance, we implement a simplistic model of tunneling in the extracellular matrix (ECM). Our experimental results show that overexpression of AQP-1 induces an increase in MMP activity which, in turn, results in ECM degradation. In our model we assume that enhanced ECM degradation results in the creation of tunnels in the ECM. We implement a very simplistic model of this tunneling mechanism by recording the history of leader positions, which we define as a "tunnel". If a follower is sufficiently close to a tunnel, then it starts moving along that tunnel towards the front of the stream. If a cell is sufficiently close to more than one tunnel, then it enters the closest tunnel. We assume that guidance via "chains" dominates the tunneling mechanism, i.e. if a follower cell is in a chain then it does not search for a tunnel.

We include phenotype switching based on the position of a cell within a migratory stream. We make a simplification from the previous model by McLennan et al. (2015a) and assume that the phenotype is determined based on cell position rather than VEGF concentration. This simplification is consistent with the experimental observation that gene expression profiles depend on the position of a cell within a migratory stream, with a small number of leaders at the very front of the stream where the concentration of VEGF is the highest (McLennan et al. 2015a). A constant number of leaders is a reasonable as-

sumption in our model because we do not model the system with experimental perturbations in VEGF distribution that have been shown to alter the number of leaders (McLennan et al. 2015b).

1.2 Model assumptions

We now list the key assumptions used in the model. Firstly, we use a fixed time-step model ($\Delta t = 1$min) during which a cell senses its environment and updates its position. Secondly, we model volume exclusion by considering cells as hard-discs that are not allowed to overlap (in reality, cells will deform when they come in contact, so this is a model simplification). If a cell cannot make a movement due to volume exclusion, i.e. the target destination is occupied by other cells, then it remains in the same position. Thirdly, we assume that only the center of the cell has to be inside the rectangular domain (Figure 7H), not the entire cell body. We allow a cell to extend filopodia outside the domain but, in our model, this never leads to a movement in that direction. If all the filopodia of a cell are extended outside the domain and the random direction sampled leads to a movement outside the domain, then the cell does not move. These are the boundary conditions for cells everywhere apart from the neural tube (x = 0) where there is an influx of cells. There is an attempt to insert a new cell at every time step with a center at a random position along the y axis and $x =$ cell radius (that is, the cell is placed fully inside the domain). Lastly, we assume that when cells enter tunnels they move in the direction towards the front of the stream, which means that we assume that there is another guidance cue in tunnels that directs the cells.

1.3 Model features

Filopodia stability, filopodia polarity, filopodia number and ECM degradation rate are new features of the model that we investigate. Filopodia stabilization is implemented here by allowing a leader to sample its environment only every three time steps and in between specifying the cell to move persistently, as opposed to sampling and potentially moving in a different direction each time step. Filopodia polarization entails a leader only stabilizing its filopodium when it makes an informed movement towards a higher concentration of VEGF, as opposed to a movement in a random direction. Filopodia number is the number of random directions a leader samples per time step. We incorporate enhanced ECM degradation by the tunneling mechanism described above, i.e. tunnels generated by the leaders correspond to enhanced ECM degradation. We consider a suite of models to explore the effects of combinations of different experimental perturbations. We label them as “Model x” (x from 1 to 11) and the values of parameters and features for the different models can be found in Table 1.

1.4 Domain

We use a rectangular two-dimensional domain $(x, y) \in [0, L_x(t)] \times [0, L_y]$ as a simplification of a narrow (in height) curved three-dimensional migratory path (Figure 1). We fit the following equation to model the growth of the domain in the x direction:

$$L_x(t) = \frac{L_\infty e^{a(t-t_s)}}{L_\infty/L_0 + e^{a(t-t_s)} - 1} + k_0, \tag{1}$$

with $a = 0.23\text{h}^{-1}\mu\text{m}^{-1}$, $t_s = 15.9\text{h}$, $L_\infty = 867.6\mu\text{m}$, $L_0 = 300.0\mu\text{m}$ and $k_0 = 291.2\mu\text{m}$ inferred from experimental results (McLennan et al. 2012).

1.5 Chemoattractant dynamics

We use a reaction-diffusion equation to model the dynamics of the chemoattractant VEGF based on the work of McLennan et al. (2012, 2015a,b, 2017). We scale the concentration of VEGF, $c(x, y, t)$, to $c \in [0, 1]$ and define the equation on the growing domain with $x \in [0, L_x(t)]$ and $y \in [0, L_y]$ (parameter values in Table 1):

$$\frac{\partial c}{\partial t} = \underbrace{D\left(\frac{\partial^2 c}{\partial x^2} + \frac{\partial^2 c}{\partial y^2}\right)}_{(1)} \underbrace{- c\sum_{i=1}^{N(t)} \frac{\lambda}{2\pi R^2} \exp\left[-\frac{(x-x_i)^2 + (y-y_i)^2}{2R^2}\right]}_{(2)} + \underbrace{\kappa c(1-c)}_{(3)} - \underbrace{\frac{\partial (ac)}{\partial x}}_{(4)}, \tag{2}$$

where D is the diffusion coefficient of the chemoattractant, R is the cell radius, λ is the internalization rate, κ is the production rate of the chemoattractant, a is the flow due to domain growth, $N(t)$ is the number of cells at time t and (x_i, y_i), $i = 1, \ldots, N(t)$ is the position of the center of cell i. We assume zero flux boundary conditions and initial conditions $c(x, y, 0) \equiv 1$. Zero flux boundary conditions are assumed to incorporate a wide and representative stream profile with no loss of chemoattractant from the system. We assume a uniform initial condition based on the observations of McLennan et al. that prior to NC migration VEGF is spatially uniform in the tissue up to the entrance to BA2 (Figure 1) (McLennan et al., 2010).

We briefly explain the reasoning behind the terms on the right-hand side of equation (10). Term (1) corresponds to diffusion of chemoattractant with diffusion coefficient D. Term (2) is the internalization of chemoattractant by cells. We use a simple Gaussian kernel because it takes into account the size of cells, and we assume that the cells consume or degrade chemical with a continually decreasing intensity moving away from the cell center. Term (3) is the production of chemoattractant. We assume logistic production, however, since the production rate, κ, is relatively small in comparison with the internalization rate, λ (see McLennan et al., 2010), the dynamics do not change significantly when other forms of production, such as linear or constant, are considered. Term (4) corresponds to the effect of domain growth. It consists of the advection term, $a \times \partial c/\partial x$, corresponding to elemental areas moving with the flow due to local growth, and a dilution term, $c \times \partial a/\partial x$, due to local area change. Assuming

that the flow can be specified using a growth function Γ, the Lagrangian description is

$$x = \Gamma(X, t), \qquad x \in [0, L_x(t)] \tag{3}$$

where X is an initial position marker, and $\Gamma(X, 0) = X$. The local flow is determined by

$$a(x, t) = \frac{\partial x}{\partial t} = \frac{\partial \Gamma}{\partial t}, \tag{4}$$

(Crampin et al., 1999). Since in our model we assume, for simplicity, that the uniform growth is in one direction (the x direction), the growth function is given

$$\Gamma(X, t) = Xl(t) = x, \qquad l(0) = 1, \tag{5}$$

where $l(t)$ is rescaled domain length, $l(t) = L_x(t)/L_0$ with $L_0 = L_x(0)$. Then the flow is determined by

$$a(x, t) = X\dot{l}(t) = x\frac{\dot{l}(t)}{l(t)}, \tag{6}$$

where $\cdot$ denotes $\mathrm{d}/\mathrm{d}t$. Substituting expression (6) into equation (2), we find

$$\frac{\partial c}{\partial t} = D\left(\frac{\partial^2 c}{\partial x^2} + \frac{\partial^2 c}{\partial y^2}\right) - c\sum_{i=1}^{N(t)} \frac{\lambda}{2\pi R^2} \exp\left[-\frac{(x - x_i)^2 + (y - y_i)^2}{2R^2}\right] + \kappa c(1 - c) - \frac{\dot{l}}{l}\left[x\frac{\partial c}{\partial x} + c\right], \tag{7}$$

We use the following transformation to map the coordinates to the unit interval

$$(x, t) \to (\bar{x}, \bar{t}) = \left(\frac{x}{l(t)}, t\right). \tag{8}$$

Under this mapping

$$\frac{\partial c}{\partial \bar{t}} = \frac{\partial c}{\partial t} + x\frac{\dot{l}}{l}\frac{\partial c}{\partial x}, \tag{9}$$

which leads to the elimination of the advective term in equation (7). Therefore, if we use the transformation (8), but for the sake of simplicity now drop the bars, then equation (7) becomes

$$\frac{\partial c}{\partial t} = D\left(\frac{1}{l(t)^2}\frac{\partial^2 c}{\partial x^2} + \frac{\partial^2 c}{\partial y^2}\right) - c\sum_{i=1}^{N(t)} \frac{\lambda}{2\pi R^2} \exp\left[-\frac{l(t)^2(x - x_i)^2 + (y - y_i)^2}{2R^2}\right] + \kappa c(1 - c) - \frac{\dot{l}(t)}{l(t)}c. \tag{10}$$

Equation (10) is valid on the fixed domain $x \in [0, L_0]$ and $y \in [0, L_y]$. Recall that we assume zero flux boundary conditions and initial conditions $c(x, y, 0) \equiv 1$.

We solve equation (10) using a finite difference method (second-order centred differences in space, and forward Euler in time) with $\Delta x = 10\mu$m, $\Delta y = 10\mu$m and $\Delta t_c = 1$min. These choices are sufficient for the algorithm to have converged and resolve accurately the gradient of VEGF. Note that a time step of 1min is equivalent to the discrete simulation time step for the cell motility model (see Table 1), which is sufficient for the simulations to converge.

1.6 Pseudocode

We provide a pseudocode that explains in detail how we numerically simulate the model. The text in blue corresponds to the steps that are only applicable for the model with a tunneling mechanism included.

The full code is available at https://github.com/rginiunaite/NC-cells.git. We provide two versions of the code: NC-model (Models 1-9), where the interactions between the cells in the NC-model are only by chains; NC-model-tunneling (Models 10,11) where interactions are by both chain and tunneling mechanisms. Note that a user first needs to install the Aboria library (https://martinjrobins.github.io/Aboria/).

Main steps

1. Initialise model parameters and insert N_{leader} leader cells at $x = R$ and equal distance apart in the y direction, set $t = 0$.
2. Choose a random position in y with $x = R$. If there is no overlap with other cells, insert a new follower cell at this position.
3. Solve chemoattractant profile.
4. Grow domain, update cell positions (multiply the position of a cell in the x direction by the ratio of current domain length over the domain length in the previous timestep).
5. Move cells.
6. Implement any phenotype switching.

Internal steps

move cells (Note that if a cell cannot move due to volume exclusion (R - radius of a cell) then the attempted movement is aborted)

1. **for** i = 1 to number of cells **do**
2. pick a cell at random without replacement
3. **if** the cell is a leader, **then**
4. **if** filopodium is stabilized and the cell has not finished moving three steps in the same direction, **then**
move a distance $\Delta t \times \nu$ in the same direction as before **end if**
5. **if** there is no filopodia stability mechanism or the cell has finished moving three steps in the same direction, **then**
6. pick n_{filo} random directions and measure chemoattractant concentration in those random direction(s) at distance l_{filo} away from the center of the cell, pick the highest concentration and set it to c_{new}, measure chemoattractant concentration at the center of the cell and set it to c_{old}
7. **if** $\frac{c_{new}-c_{old}}{\sqrt{c_{old}}} \geq \xi$ (sensing accuracy), **then**
8. move in chosen direction a distance $\Delta t \times \nu$, stabilize filopodium (if stabilization mechanism is on)
9. **end if**
10. **else**
11. move in random direction a distance $\Delta t \times \nu$, stabilize filopodium (if stabilization

mechanism is on and the stabilization is non-polar)
12. **end if**
13. **end if**
14. record the position of a leader if the cell is a distance s apart from the previous position tracked and less than n_t positions are recorded, define it as a "tunnel"
15. **end if**
16. **else** (the cell is a follower)
17. **if** the cell is in a chain, **then**
18. move a distance $\Delta t \times ratio \times \nu$ in the same direction as the leader at the front of the chain
19. **if** the cell is further away than l_{filo}^{max} from the cell which it was following, **then**
20. detach it, and all the cells that were following it, from the chain
21. **end if**
22. **end if**
23. **if** the cell is not in a chain, **then**
24. **if** there is a leader or a follower in a chain less than l_{filo} distance away, **then** join that chain (if there are multiple possibilities, pick one randomly) and move a distance $\Delta t \times ratio \times \nu$ in the same direction as the cell ahead in the chain
25. **end if**
26. **else if** the cell is less than threshold distance d from one of the tunnels (if there are multiple tunnels, pick the closest), **then** move a distance $\Delta t \times ratio \times \nu$ along the tunnel **end if**
27. **else** move a distance $\Delta t \times ratio \times \nu$ in a random direction
28. **end if**
29. **end for**

phenotype switching

1. **if** a cell is a follower **then**
2. **if** the cell is further ahead by ϵ in the x direction than one of the leaders and it is sufficiently close to that leader, **then** swap their phenotypes **end if**
3. **end if**

1.7 Model parameters

We choose most of our parameters based on those from McLennan et al. (2015a,b, 2017). We adapt some of the parameters to recapitulate the experimental results for the control case (Model 1), AQP-1 overexpression (Model 2) and AQP-1 downregulation (Model 3). Table 1 contains the values we used

for the computational results of this paper.

Comments

- We use a fixed-jump-length process where the length of the jump is $\Delta t \times \nu$ for leaders and $\Delta t \times ratio \times \nu$ for followers.
- N_{leader} - number of leaders. We choose a fixed number of five leaders because we find that this is the smallest number of cells that can guide the rest of the population successfully (either by chains or tunnels, results not shown). A higher number of leader cells could be chosen provided that we adjust the internalization rate, the sensing accuracy and the diffusion coefficient to avoid some leaders getting stuck due to the lack of a gradient of chemoattractant.
- $ratio$ - ratio of follower to leader speed. Kulesa et al. (2008) demonstrated that the speed of the followers is higher than that of the leaders. We chose a *ratio* value sufficiently high to ensure that the stream does not break in the control case.
- l_{filo} - sensing radius. We use the value calculated by McLennan et al. (2015) as the sum of the cell radius and the mean filopodial length.
- l_{filo}^{max} - maximum cell separation before contact is lost. We use the value calculated by McLennan et al. (2015), obtained from half of the maximum cell size including filopodium.
- ξ - sensing accuracy. We use the same argument for the accuracy with which the cells can sense a chemical gradient as McLennan et al. (2012, 2015, 2015, 2017). They base their work on the biophysical limit for sensing accuracy derived by Berg and Purcell (1977). Briefly, they assume that fluctuations in molecule number are proportional to $\sqrt{N}$, where N is molecule number. Since we use a continuum variable for the chemoattractant, fluctuations can be expressed as $\sqrt{Ac}$ where A is some area of interest, and c is the average concentration in that area. The inaccuracy of concentration measurements is inversely proportional to fluctuations, which gives

$$\frac{\Delta c}{c} \approx \frac{1}{\sqrt{N}} = \frac{1}{\sqrt{Ac}}. \tag{11}$$

  Rearranging gives

$$\frac{\Delta c}{\sqrt{c}} \approx \xi, \tag{12}$$

  where we define ξ as the sensing accuracy, and $\Delta c = c_{new} - c_{old}$. $\Delta c/\sqrt{c_{old}}$ has to be greater or equal than ξ for the cell to respond. We choose ξ sufficiently high to ensure that movement does not occur in response to very small changes in VEGF concentration. The results are robust if we change this parameter together with the internalization rate λ.
- D - diffusion coefficient of chemoattractant. The exact value of the diffusion coefficient is unknown for the system. We use a relatively small value because it has been shown that only around 1% of VEGF freely diffuses, whilst the rest binds to the ECM (Mac Gabhann et al. 2006). The results are robust to changes in this parameter because it only affects the sharpness of the gradient of VEGF.

Changes in the internalization rate, λ, and the sensing accuracy, ξ, also influence the choice of the diffusion coefficient.

- χ - production rate of chemoattractant. The exact VEGF production rate in the tissue is unknown, but since experimental results show that there is almost no VEGF produced where the cells have already internalized it (McLennan et al. 2010), we assume that the production rate is small.

- λ - chemoattractant internalization rate. The internalization rate is also unknown, we choose this parameter based on the distance traveled by cells in 24h. The results are robust to simultaneous changes in the sensing accuracy, ξ, and the internalization rate, λ, therefore we adapted the internalization rate to our chosen sensing accuracy, ξ.

- ϵ - distance a follower has to be ahead of a leader to swap phenotypes. As discussed in Section 1.4, we use a simplified version of the switching mechanism based on the position in the stream. We assume that a follower has to be $\epsilon = 10\mu$m ahead of a leader for their phenotypes to swap. The results are robust to changes in this parameter because we have a fixed number of leaders.

- d - threshold distance to tunnel to enter it. This parameter has to be chosen carefully with respect to the distance between leader positions that we record, s. It is advisable that d is at most $s/2$, so that a cell is not too close to two tunnel positions at the same time, in which case it randomly chooses which one to start moving along. However, it is unrealistic to choose $d \ll 10\mu$m because we need to incorporate the width of a tunnel.

- s - track spacing. This is a parameter that determines the distance between leader positions that we record, corresponding to a "tunnel". We choose a small value to represent a continuous tunnel on a scale of cell sensing, but not too small to avoid high computational costs. The model is robust to smaller values of s ($s < 20\mu$m), but not for significantly larger values.

- n_t - number of leader positions tracked. We have to choose this parameter sufficiently large so that tunnels extend along the entire domain. We find that if a tunnel is shorter than the length of the domain, then the likelihood of the stream to break is increased.

References

Robinson, M. and Bruna, M. (2017). *Particle-based and meshless methods with Aboria.* SoftwareX, 6:172 – 178.

Crampin E. J., Gaffney E. A., and Maini P. K. (1999). *Reaction and diffusion on growing domains: scenarios for robust pattern formation.* Bulletin of Mathematical Biology, 61(6):1093-1120

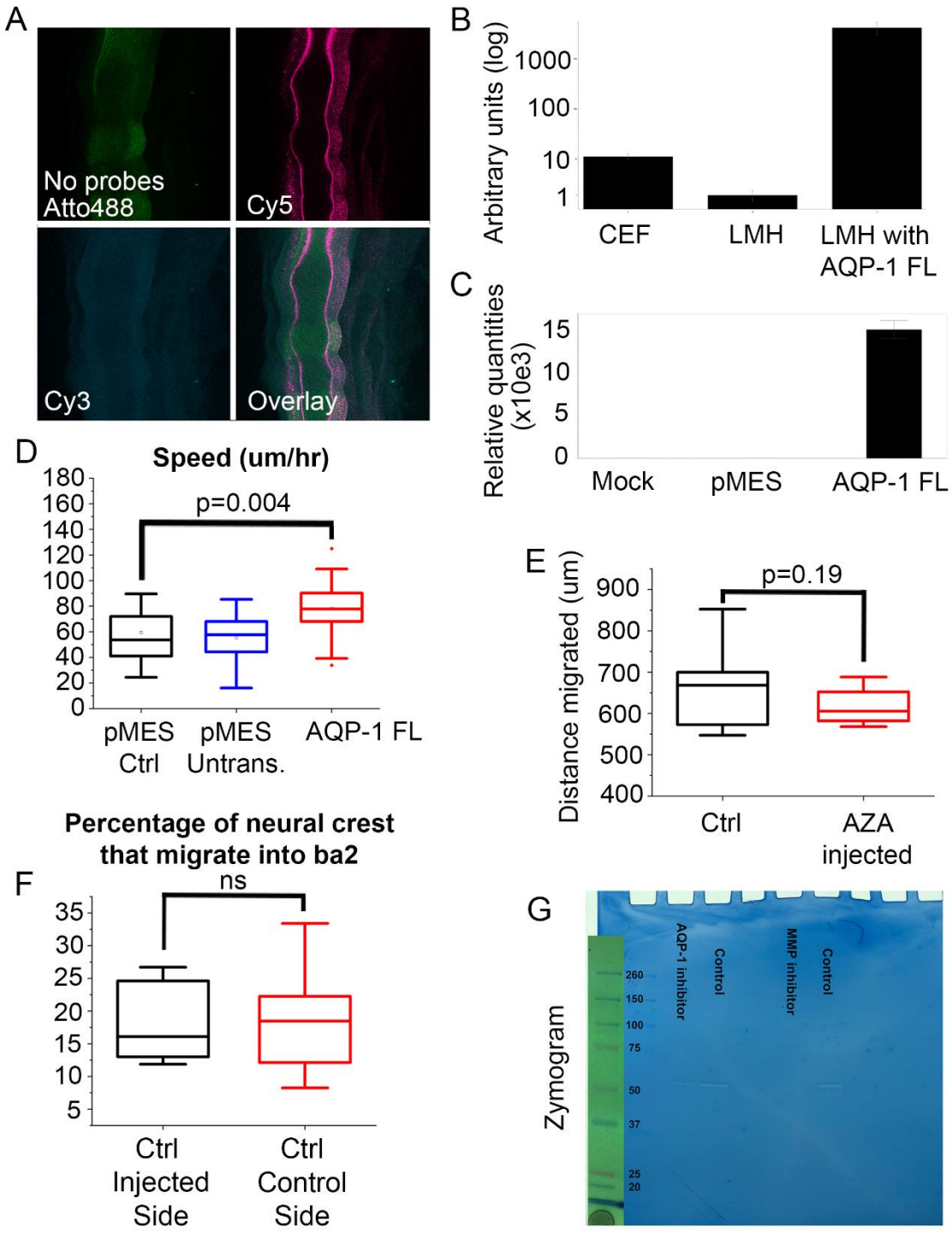

Figure S1. (A) No probes control for RNAscope experiment. (B) Quantification of AQP-1 RNA expression in chick embryonic fibroblasts (CEF), chick liver hepatocellular carcinoma (LMH) and LMH transfected with AQP-1 FL. (C) Quantification of AQP-1 RNA expression in LMH cells after mock transfection, pMES transfection and AQP-1 FL transfection. (D) Box plot of the Speed (microns/hr) of neural crest cells, transfected with pMES control vector (black, n= 27 cells from n=9 neural tube explants), non-transfected but in the same cultures as pMES (blue, n=26 cells) and transfected with AQP-1 FL in different cultures but prepared and imaged the same days as controls (red, n=33 cells from n=10 neural tube explants). (E) Box plot of the distance migrated by neural crest cells after mesodermal injections of AZA (red) and the distance migrated by neural crest cells on the control sides of the same embryos (black), n=6 embryos. (F) Box plot of the percentage of neural crest cells that migrate into the branchial arches, n=8 embryos per treatment. (G) The entire zymogram that is quantified in Figure 5. An image of the ladder (left) was taken prior to development so that it could be clearly seen. Proteins in these assays do not run exactly the same as the markers as enzymes in the samples are not reduced while the markers are (Woessner, 1995). The band size is approximately 62 kD, corresponding to MMP2 (Anderson, 2010).

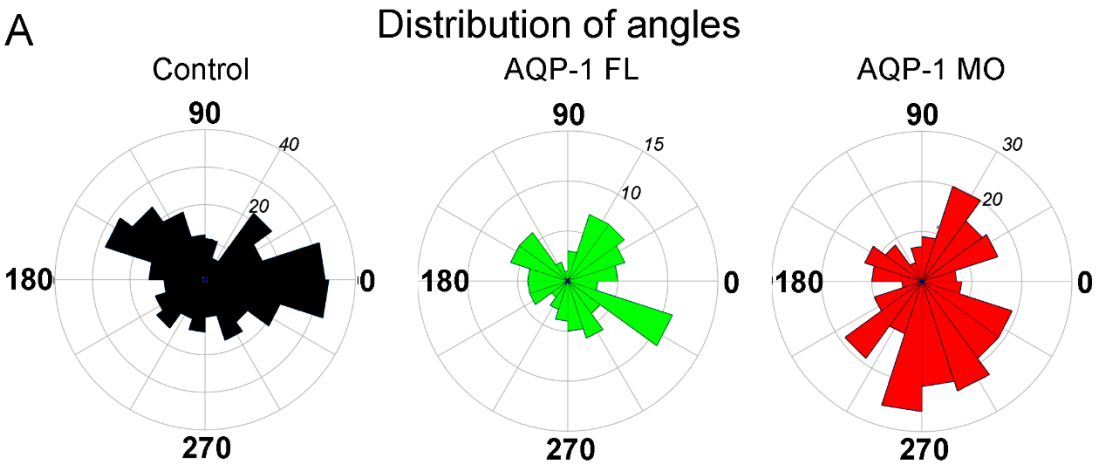

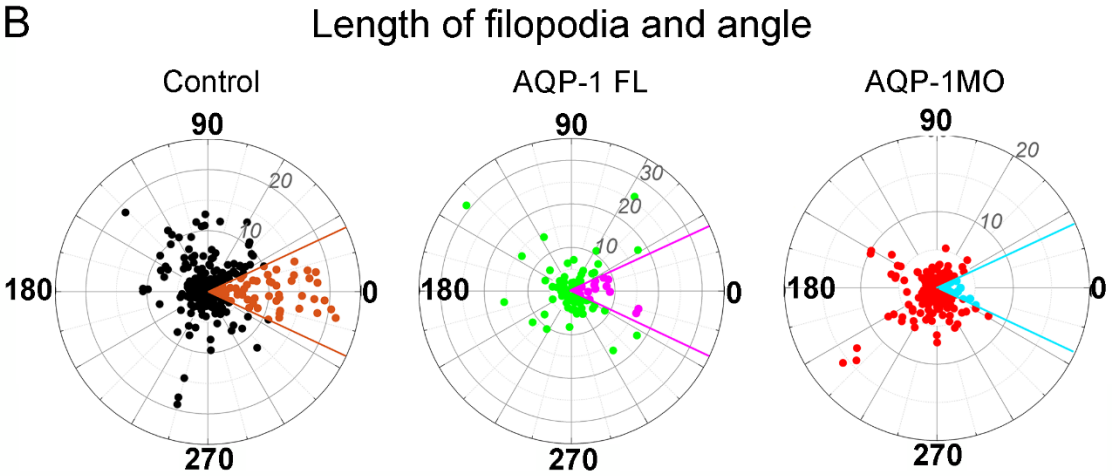

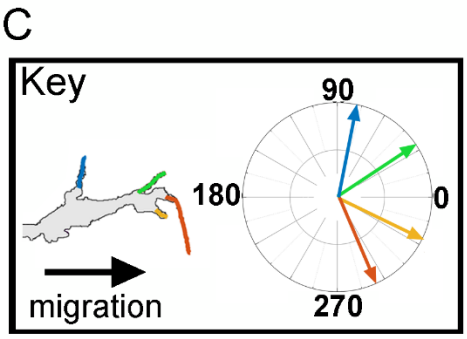

Figure S2: Filopodia direction and length with respect to neural crest migratory direction. (A) Distribution of angles of filopodia for control (black), AQP-1 FL overexpression vector (green) and the AQP-1 MO (red) labeled cells. Radial magnitude equals number of filopodia in that direction. (B) Length and direction of the filopodia for cells labeled with control vector, AQP-1 FL overexpression vector or AQP-1 morpholino. Radial magnitude equals length of the filopodia in microns and angle is with respect to migratory direction. Contrasting colored filopodia are in a 30° window around the direction of migration. (C) Example neural crest filopodia with direction of migration indicated. Direction of migration is always set to 0 degrees.

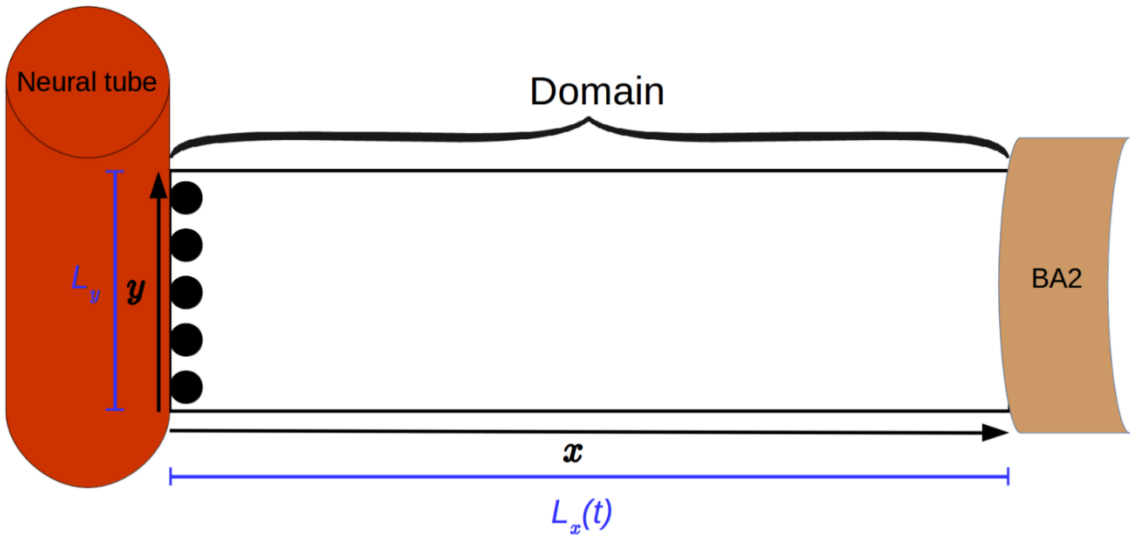

Figure S3: Schematic of a rectangular domain we used to model the domain on which the neural crest cells migrate (black circles). They enter the domain from the neural tube (x = R). BA2 denotes branchial arch 2.

Table S1: Genes that are differentially expressed between pMES (control) and AQP-1 FL.

Click here to Download Table S1

	Description	**Value**	Reference
N_{leader}	number of leaders	5	comments
n_{filo}	directions sampled per time step, filopdia number	1-3	results section
Δt	simulation time step, min	1	n/a
R	cell radius (nuclear), μm	7.5	McLennan and Kulesa (2010)
ν	leader cell speed, μm/h, control case, AQP-1 overexpression and AQP-1 downregulation, respectively	62, 82, 57	results section
$ratio$	ratio of follower to leader speed	1.3	comments
L_y	width of migratory domain, μm	120	McLennan et al. (2012)
$L_x(t)$	length of migratory domain (grows based on eq. (1)), μm	300 to 1100	McLennan et al. (2012)
	Parameters for domain growth equation (1)		
a	growth parameter, h$^{-1}\mu$m^{-1}	0.23	Section 1.1
t_s	growth parameter, h	15.9	Section 1.1
L_∞	growth parameter, μm	867.6	Section 1.1
L_0	initial length of the domain, μm	300	Section 1.1
k_0	growth parameter, μm	291.2	Section 1.1
l_{filo}	sensing radius, μm	27.5	comments
l_{filo}^{max}	maximum cell separation before contact is lost, μm	45	comments
ξ	sensing accuracy	0.1	comments
D	diffusion coefficient of chemoattractant, μm^2/h	0.6	comments
κ	production rate of chemoattractant, /h	0.006	comments
λ	chemoattractant internalization rate, μm$^2/h$	0.02	comments
ϵ	distance a follower has to be ahead of a leader to swap phenotypes, μm	10	comments
	Extra parameters for model with tunneling (Models 10 and 11)		
d	threshold distance to tunnel to enter it, μm	10	comments
s	track spacing, μm	20	comments
n_t	number of leader positions tracked	60	comments

Table S2: Model parameters used in the simulations provided in the results section.

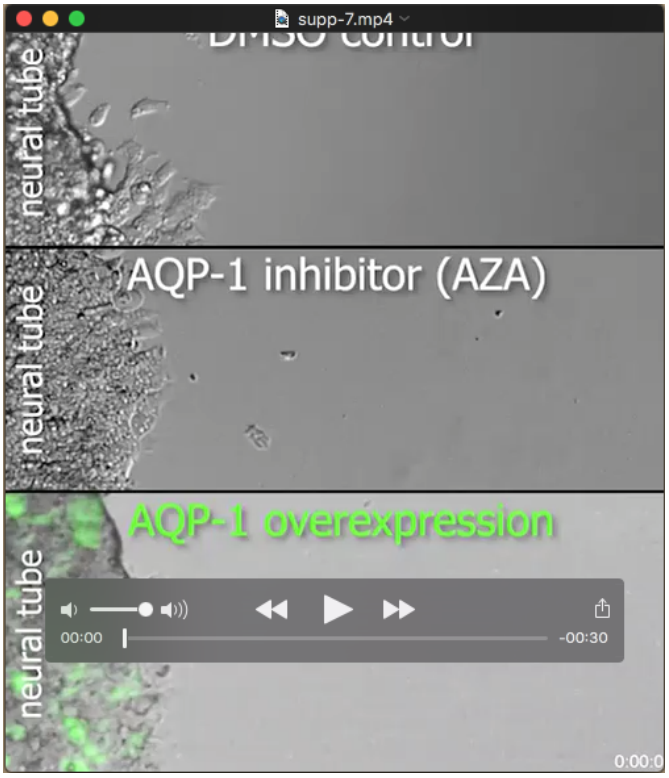

Movie 1: Cranial neural crest cell migratory behaviors are altered in vitro after AQP-1 manipulation. (top) Control migrating neural crest cells exposed to DMSO. (middle) AQP-1 was inhibited by adding Acetazolamide (AZA) to the media. AZA was solubilized in DMSO. (bottom) AQP-1 was overexpressed by transfection of AQP-1 full length construct (green cells). Cranial neural tube explants are shown on the left-hand side of each panel. Time intervals between images ranged from 2.5 to 4 minutes and frame speed was adjusted so that each time-lapse was 8 hours in duration. Scale bar= 30 um.

Movie 2: Cranial neural crest cell migratory behaviors are altered in vivo after AQP-1 manipulation. (Left) Premigratory neural crest cells were transfected with Gap43-YFP/H2B mCherry (control). (Right) AQP-1 full length/H2B mCherry. Z-stacks were collected every 5 minutes and approximately 6 hours is shown. Scale bar= 20 um.

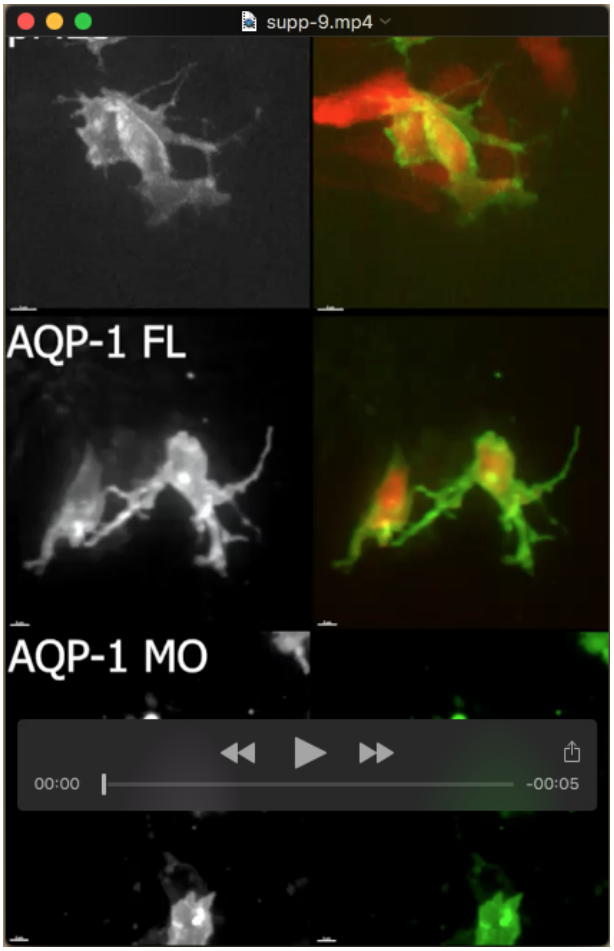

Movie 3: Fast confocal imaging reveals changes in neural crest cell filopodial dynamics after AQP-1 manipulation. Projected images from spinning disk time-lapse microscopy of migrating lead neural crest cells in whole embryo culture electroporated with either (top) pMES control, (middle) AQP-1 FL or (bottom) AQP-1 Morpholino (MO). Each movie sequence shows the cell membrane label (Gap43-mTurquoise2) to highlight the cell protrusion dynamics. Images were collected in 30 second intervals and shown here for approximately 11 min.

Movie 4: Cranial neural crest cell directionality is altered after AQP-1 manipulation. Premigratory neural crest were transfected with pMES (control) or AQP-1 FL and neural tubes were plated in the presence of branchial arch 2 (ba2) tissue as a source of known endogenous chemoattraction. Images were collected every 5 minutes and a total of approximately 18 hours of elapsed time is shown. Scale bar= 50 um.

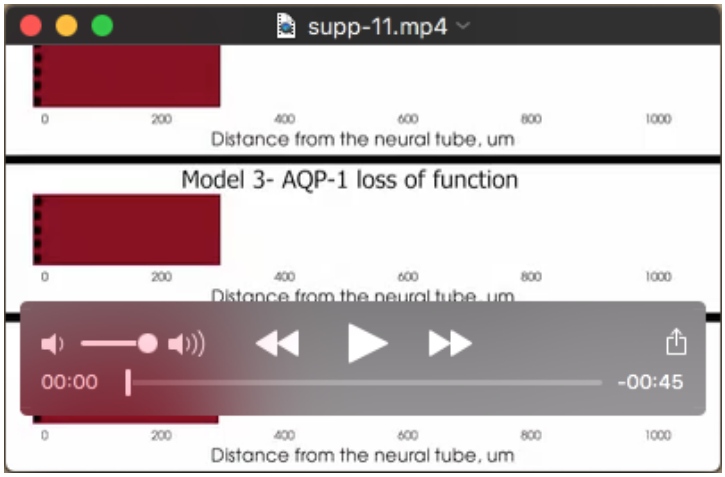

Movie 5: Computer model simulations of cranial neural crest cell migration with AQP-1 manipulation. (top) Control migration is modeled by normal cell speed and unstable filopodia. (middle) AQP-1 loss-of-function is modeled by reduced cell speed and reduced number of cell filopodia. (bottom) AQP-1 gain-of-function is modeled by increased cell speed, stable cell filopodia and tunneling. Each simulation is run on a 2D migratory domain.